

# Journal of Materials Chemistry A

Accepted Manuscript



This is an *Accepted Manuscript*, which has been through the Royal Society of Chemistry peer review process and has been accepted for publication.

*Accepted Manuscripts* are published online shortly after acceptance, before technical editing, formatting and proof reading. Using this free service, authors can make their results available to the community, in citable form, before we publish the edited article. We will replace this *Accepted Manuscript* with the edited and formatted *Advance Article* as soon as it is available.

You can find more information about *Accepted Manuscripts* in the [Information for Authors](#).

Please note that technical editing may introduce minor changes to the text and/or graphics, which may alter content. The journal's standard [Terms & Conditions](#) and the [Ethical guidelines](#) still apply. In no event shall the Royal Society of Chemistry be held responsible for any errors or omissions in this *Accepted Manuscript* or any consequences arising from the use of any information it contains.

## Degradation observations of encapsulated planar CH<sub>3</sub>NH<sub>3</sub>PbI<sub>3</sub> perovskite solar cells at high temperatures and humidity

Cite this: DOI: 10.1039/x0xx00000x

Received 00th January 2012,  
Accepted 00th January 2012

DOI: 10.1039/x0xx00000x

www.rsc.org/

Yu Han,<sup>a</sup> Steffen Meyer,<sup>b</sup> Yasmina Dkhissi,<sup>c</sup> Karl Weber,<sup>d</sup> Jennifer M. Pringle,<sup>e</sup> Udo Bach,<sup>d,f</sup> Leone Spiccia,<sup>b,\*</sup> and Yi-Bing Cheng<sup>a\*</sup>

The stability of encapsulated planar-structured CH<sub>3</sub>NH<sub>3</sub>PbI<sub>3</sub> (MAPbI<sub>3</sub>) perovskite solar cells (PSCs) was investigated under various simulated environmental conditions. The tests were performed under approximately one sun (100 mW/cm<sup>2</sup>) illumination, varying temperature (up to 85 °C cell temperature) and humidity (up to 80%). The application of advanced sealing techniques improved the device stability, but all devices showed significant degradation after prolonged aging at high temperature and humidity. The degradation mechanism was studied by post-mortem analysis of the disassembled cells using SEM and XRD. This revealed that the degradation was mainly due to the decomposition of MAPbI<sub>3</sub>, as a result of reaction with H<sub>2</sub>O, and the subsequent reaction of hydroiodic acid, formed during MAPbI<sub>3</sub> decomposition, with the silver back contact electrode layer.

### Introduction

CH<sub>3</sub>NH<sub>3</sub>PbI<sub>3</sub> (MAPbI<sub>3</sub>) perovskite solar cells (PSCs) have reached a certified efficiency of 20.1% in 2014,<sup>1,2</sup> up from 3.81% reported in 2009,<sup>3</sup> making them a promising alternative to conventional thin film solar cells. These PSCs can be assembled as mesoscopic or planar structured devices. Originally, the mesoscopic structured PSCs were made using a one-step precursor deposition method,<sup>4</sup> which led to uncontrolled morphology of perovskite films and large variations in cell efficiency. A sequential deposition method was then introduced to control the morphology of the perovskite film. This led to a better reproducibility of device performance and efficiencies exceeding 15%.<sup>5</sup> In subsequent studies, various innovative cell fabrication techniques were developed to produce planar structured PSCs with high photovoltaic conversion efficiencies: 15.4% by dual-source vapour deposition<sup>6</sup>, 12.1% by vapour-assisted solution process<sup>7</sup>, 13.7% by low-temperature solution casting<sup>8</sup>, and 13.9% by a solvent-induced fast crystallization method<sup>9</sup>. Recently, a gas assisted preparation method was developed by our group and the cells fabricated by this method demonstrated an average efficiency of 15.7%<sup>10</sup>.

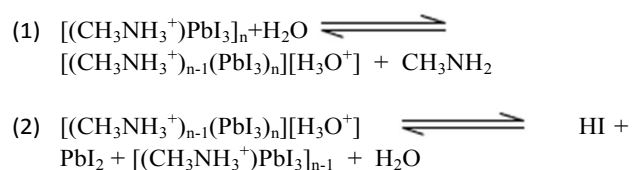
Despite the major improvements in device efficiency and fabrication methods made over the last few years,<sup>11–16</sup> one of the most significant concerns for PSCs is their long-term stability.<sup>5</sup> So far, few investigations have focused on the encapsulation, stability and degradation mechanisms of PSCs.

In 2013, Burschka *et al.* reported a 15% efficiency mesoscopic MAPbI<sub>3</sub> perovskite solar cell made by the sequential deposition method that showed very promising long-term stability.<sup>15</sup> The device was sealed under argon and maintained more than 80% of its initial photoelectric conversion efficiency (PCE) after a period of 500 h continuous operation at 45 °C at its maximum power point under a light intensity of approximately 100 mW cm<sup>-2</sup>. The efficiency decline was mainly due to a decrease in the shunt resistance that caused a lower  $V_{oc}$  and  $FF$ . Later, Leijtens *et al.* demonstrated that a CH<sub>3</sub>NH<sub>3</sub>PbI<sub>3-x</sub>Cl<sub>x</sub> PSC with a mesoporous Al<sub>2</sub>O<sub>3</sub> scaffold can overcome UV induced instability. The cells were encapsulated with an epoxy resin and a glass coverslip in a nitrogen-filled glove box. Their devices showed only a small decrease in photocurrent over 1,000 h under continuous full spectrum AM1.5 solar illumination at 40 °C.<sup>17</sup> However, a 50% drop in efficiency occurred primarily during the initial 200 h of aging. This was again mainly due to a decrease of  $V_{oc}$  and  $FF$ .<sup>17</sup> The authors also pointed out that the silver charge collecting electrode could corrode when in contact with the perovskite layer, possibly forming silver halide.<sup>17</sup> Noh *et al.* found that the substitution of larger iodide ions with smaller bromide ions in the CH<sub>3</sub>NH<sub>3</sub>Pb(I<sub>1-x</sub>Br<sub>x</sub>)<sub>3</sub> material with  $x \geq 0.2$  led to a greater resistance towards high humidity ( $\geq 55\%$ ) at room temperature.<sup>18</sup> It was postulated that bromide doping leads to a more compact and stable perovskite structure due to a reduction of the lattice constants and the transition to a cubic phase.<sup>18</sup> Li *et al.* demonstrated that CH<sub>3</sub>NH<sub>3</sub>PbI<sub>3</sub> could be

corroded by 4-*tert*-butylpyridine (4-tBP) which is an important additive in the Spiro-OMeTAD hole transporting material.<sup>19</sup> The corrosion was proposed to occur because 4-tBP was able to dissolve the  $\text{CH}_3\text{NH}_3\text{PbI}_3$  and form complexes of the type,  $[\text{PbI}_2(4\text{-tBP})_x]$ . To protect the perovskite, a montmorillonite (MMT) layer was introduced between the perovskite and Spiro-OMeTAD layers, but long-term durability test results were not reported.<sup>19</sup>

Most recently, an unsealed device with approximately 11.5% initial PCE was reported by Mei *et al.* which showed excellent stability under AM 1.5 simulated sunlight.<sup>20</sup> The authors produced a device without a hole transporting layer, using a modified perovskite material  $(5\text{-AVA})_x(\text{MA})_{(1-x)}\text{PbI}_3$  and a carbon counter electrode. They proposed that the observed stability over 1000 h, with almost no drop in photovoltaic conversion efficiency, was due to the perovskite being protected by the thick carbon layer,<sup>20</sup> but the tests were done in ambient conditions.

In all previous studies, the degradation of the perovskite layer was attributed to a reaction with water from the atmosphere. Recently, Frost *et al.* proposed a plausible decomposition pathway for  $\text{MAPbI}_3$  in the presence of water.<sup>21</sup> The authors suggested that water catalyses the decomposition of  $\text{MAPbI}_3$  through the reversible reactions (1) & (2) shown below:



Hydroiodic acid has a boiling point of  $-35.4\text{ }^\circ\text{C}$ <sup>22</sup> and methylamine of around  $-6\text{ }^\circ\text{C}$ <sup>23</sup>, thus both exist in the gas phase at room temperature. In an open system, the continuous release of these gases can drive the decomposition reaction forward and, according to the proposed mechanism, even a small amount of water is sufficient to degrade the perovskite material. The above studies are only the first steps on the road to meeting the stringent international standards for outdoor photovoltaic applications.<sup>24</sup> As the normal operational environment for photovoltaic devices is under direct sunlight, the cell temperature can be up to  $45\text{ }^\circ\text{C}$  higher than the environmental temperature.<sup>25</sup> Thus, if, for example, the environmental temperature is  $40\text{ }^\circ\text{C}$ , the device temperature can be as high as  $85\text{ }^\circ\text{C}$ . Moreover, daily temperature fluctuations can be as high as  $45\text{ }^\circ\text{C}$  even in mild environmental conditions.<sup>26</sup> Inevitably, this also increases the demand for high mechanical stability of the devices during thermal expansion and contraction. Furthermore, solar cells can become exposed to moisture from atmospheric humidity and rain. Thus, it is critical to fully encapsulate the devices to achieve good stability at high temperatures in the presence of moisture.

Here, we report a study on the encapsulation, stability and degradation of planar structured PSCs under a number of different environmental conditions, including varying temperature and humidity, under approximately one sun

simulated light intensity. The solar cells were dismantled after the stability tests to investigate the degradation pathways.

## Experimental

### Cell Fabrication, Sealing and Performance

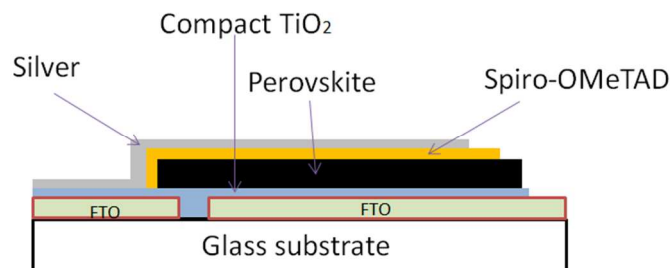


Figure 1. Schematic cross-section of the planar perovskite solar cell

The structure of the fabricated perovskite solar cells is shown in Figure 1. The gap in the FTO layer was produced by laser ablation, so that the right side of the substrate acted as the photoanode and the left side of the substrate, which was connected to the silver layer, acted as the photocathode. On top of the FTO coated glass substrate, after the laser cutting and glass cleaning with surfactant and ethanol, a thin 30 nm compact  $\text{TiO}_2$  layer was deposited by spray pyrolysis of a diisopropoxide bis(acetylacetonato) titanium(IV) solution at  $450\text{ }^\circ\text{C}$ . The perovskite layer, *ca.* 400 nm in thickness, was produced by the gas-assisted deposition technique and subsequent annealing at  $100\text{ }^\circ\text{C}$  for 10 min according to the method recently developed in our laboratory.<sup>10</sup> The hole transporting layer, *ca.* 300 nm in thickness, was deposited by spin coating a solution of Spiro-OMeTAD (41.6 mg) in chlorobenzene (0.5 mL), with 3.72 mg lithium bis(trifluoromethanesulfonyl)imide (LiTFSI) and 12.1  $\mu\text{L}$  4-tBP as additives, at a speed of 3000 rpm for 30 s. Both the deposition of perovskite layer and Spiro-OMeTAD layer was performed in a glove box under a dinitrogen atmosphere. Finally, an 80 nm silver layer was deposited as the back contact by thermal evaporation under vacuum.

To test the stability of the perovskite solar cells under simulated environmental conditions, two sealing configurations were applied, as illustrated in Figures 2 and 3. Sealing method A used a UV-curable epoxy resin from Epotek (3035B) that was filled between the silver counter electrode and a plain glass cover. Sealing method B is a more advanced encapsulation technique adopted from the organic light emitting diode (OLED) technology. This technique was chosen as OLED materials are also very sensitive to moisture. The encapsulated device consists of a cover glass from HanaAMT with a recess in the middle to accommodate a  $10 \times 15\text{ mm}$  piece of desiccant from Dynic (HG sheet of  $180\text{ }\mu\text{m}$  in thickness). The purpose of this absorber is to adsorb water that has permeated through the UV epoxy sealing during long-term operation under simulated atmospheric conditions. The UV-curable epoxy adhesive used for sealing was purchased from Nagase ChemTex (XNR5516Z-

B1), and is specifically designed for OLEDs and has a low water vapour transmission rate of around  $3 \times 10^{-4}$  g/m per day according to the manufacturer. The sealing of the devices was performed in a glove box under a dinitrogen atmosphere with less than 0.1 ppm oxygen and moisture.

Perovskite solar cell devices fabricated by the gas-assisted deposition technique have previously achieved PCEs of  $15.7 \pm 0.7\%$ .<sup>10</sup> In this work, it was found that the encapsulation processes reduced the cell efficiency significantly, possibly due to a lack of dioxygen doping of the Spiro-OMeTAD layer as both the device fabrication and encapsulation procedures were carried out in an inert atmosphere,<sup>27</sup> and/or a reaction of the perovskite material with vapours outgassing from the UV epoxy during the UV-curing procedure. Thus, the stability studies were performed on devices with an initial average PCE of around 12%.

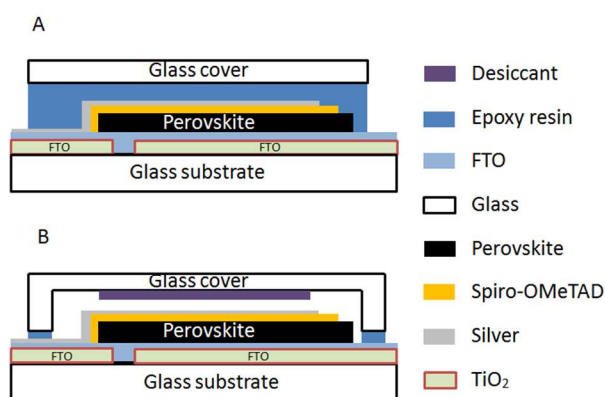


**Figure 2.** Schematic cross-section of the perovskite solar cells sealed according to technique A (top) and B (bottom).

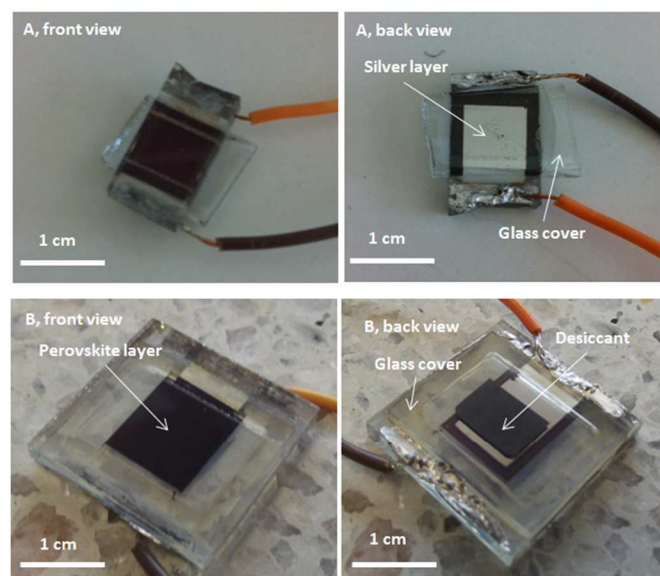


**Figure 3.** Photographs of solar cells sealed by method A (top) and B (bottom).

### Scanning Electron Microscopy (SEM) images and X-ray diffraction (XRD) patterns

The surface and cross sectional SEM images were recorded with a FEI Nova dual beam, focused ion beam (FIB), SEM instrument using 5kV acceleration voltage. Prior to ion beam thinning of the cross section, two platinum protecting layers were deposited in situ using an electron beam source at 6.3 nA and an ion beam source at 0.30 nA. The milling of the cross sections was performed with a gallium ion source at a 52° tilting angle. An X-ray diffractometer (XRD, Philips 1140) with Cu K $\alpha$  radiation was utilized to compare the crystalline structures of various new and aged devices, illustrated in Figure 10, with a scan rate of  $1^\circ \text{ min}^{-1}$  and a step size of  $0.02^\circ$ .

### Environmental Stability Testing Conditions

Stability testing was conducted using an ATLAS Environmental Chamber (SC 340 MHG), which enables a controlled temperature range of  $-20^\circ \text{C}$  to  $100^\circ \text{C}$ , relative humidity between 0% to 80% and uses a 1200 W metal halide lamp that gives approximately one sun illumination constantly during the entire testing period. The output of the halide lamp was regulated to yield short circuit currents that are comparable to the values measured using a Xe solar simulator for a standard Si solar cell. The solar cells were kept inside the chamber at open circuit, with a  $0.16 \text{ cm}^2$  circular aperture on top to define the illuminated area. A K-type thermocouple was directly attached to one solar cell of each batch to monitor the actual cell temperature during testing. During illumination, the actual cell temperature was found to be approximately  $30^\circ \text{C}$  higher than the environmental temperature inside the chamber. For the ease and clarity of discussion in the following sections, the temperatures are always presented as “environmental temperature (actual cell temperature)”, e.g.,  $55^\circ \text{C}$  ( $85^\circ \text{C}$ ). The environmental temperature, actual cell temperature and photovoltaic performances of the devices ( $V_{oc}$ ,  $J_{sc}$ ,  $FF$  and PCE) were continuously monitored and recorded every 5 minutes using an automated external  $I$ - $V$  recording instrument (National Instruments PXIe-1078).

The stability testing conditions were designed to closely follow a consensus of the stability testing protocols for organic photovoltaic materials and devices.<sup>28</sup> Cells sealed by method A were tested under three different environmental conditions:

- i. constant temperature  $-20^\circ \text{C}$  ( $10^\circ \text{C}$ ), 0% relative humidity, one sun continuous illumination;
- ii. constant temperature  $55^\circ \text{C}$  ( $85^\circ \text{C}$ ), 10% relative humidity, one sun continuous illumination;
- iii. constant temperature  $55^\circ \text{C}$  ( $85^\circ \text{C}$ ), 80% relative humidity, one sun continuous illumination.

Cells sealed by method B were then tested and compared with cells sealed by method A under *environmental condition (iii)*. Further stability testing of cells sealed by method B under *environmental condition (iv)* was then conducted for over 500 hours:

- iv. constant temperature  $55^\circ \text{C}$  ( $85^\circ \text{C}$ ), 50% relative humidity, one sun continuous illumination.

### Results and discussion

### Device Stability

The stability of the  $\text{CH}_3\text{NH}_3\text{PbI}_3$  perovskite solar cells sealed by method A was examined under three different environmental conditions (i, ii and iii). The tests were relatively short, around 120 h, but showed clear differences in device stability (Figure 4A). In the early stage of aging (< 20 h) under condition (i) and (ii), the cells showed slightly improved PCEs with the improvement more pronounced under condition (ii). This might be induced by a reduction of the number of defects in the  $\text{CH}_3\text{NH}_3\text{PbI}_3$  film with aging or further annealing<sup>29</sup> as the process was found to be faster at higher temperature. In comparison, the cells were the most stable and showed almost no photodegradation at low temperature and low humidity conditions (*condition (i)*), less stable at higher temperatures and low humidity conditions (*condition (ii)*) and the least stable at high temperature and high humidity conditions (*condition (iii)*). At 55 °C (85 °C), 80% relative humidity and one sun illumination, the devices sealed by method A lasted less than 20 h. The cell temperature for both tests at *conditions (ii)* and (*iii*) were above the phase transition temperature of  $\text{MAPbI}_3$ .<sup>30</sup> However, the significant difference between the results obtained under test *conditions (ii)* and (*iii*) indicates that environmental humidity has a stronger impact on the device stability than temperature (comparison between *conditions (i)* and (*ii*)), even above the phase transition temperature. The phase transition at around 60°C might have an effect on stability, but a conclusion cannot be drawn from our experimental design. Moisture is a major factor for the device degradation and better sealing is required to improve its environmental stability. The more sophisticated sealing method B showed an improved stability under the same *condition (iii)*, due to better encapsulation and the presence of a desiccant that reduces water vapour ingress and in turn reaction with  $\text{MAPbI}_3$  (Figure 4B), but a significant degradation was still observed within the first 4h.

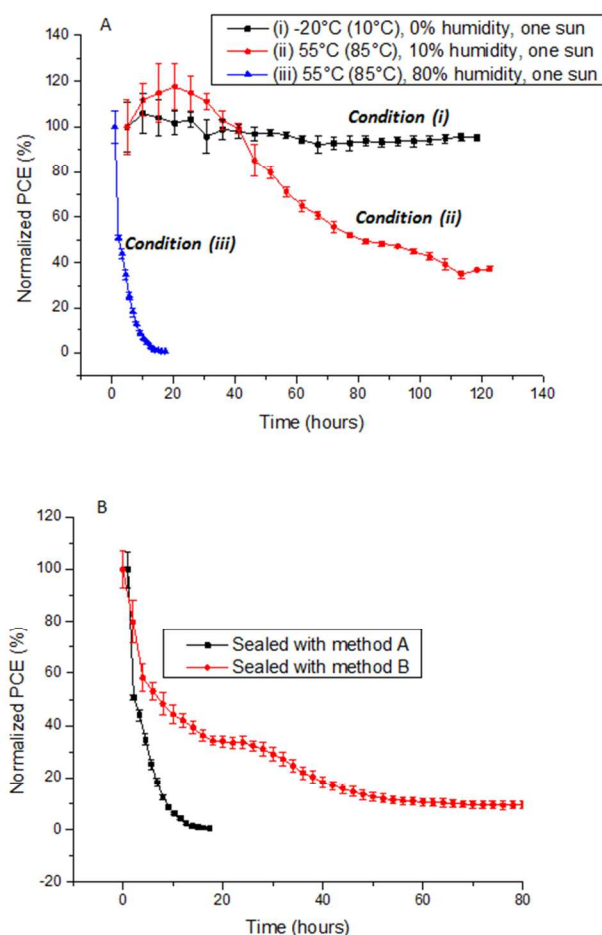


**Figure 4.** (A) Stability testing of perovskite solar cells sealed by method A under three different environmental conditions; (B) Comparison of the stability of devices sealed by method A and B and tested under *environmental condition (iii)*. The efficiency of the devices before the test was set as 100% and the results were all normalized and plotted against the initial efficiency. Three devices were averaged for each test and the error bars show the standard deviation.

Visual inspection of the tested cells sealed by method A (Figure 5), compared to the new device in Figure 3A, showed that the middle part of the cell tested under *condition (iii)* was intact while the surrounding area was significantly degraded and had turned yellowish, probably because of the formation of  $\text{PbI}_2$ . Moreover, the edges of the silver layer were damaged (Figure 5). This suggested that degradation primarily occurred as a result of ingress of moisture from the environment. Glass is impermeable to water, but the edges of the sealed device are most vulnerable to moisture.

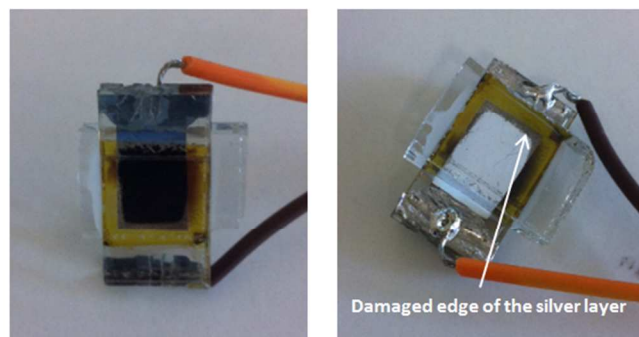


**Figure 5.** Front and back photographs of a perovskite solar cell sealed by method A after 120 h illumination at approximately one sun, 55 °C (85 °C) and 80% relative humidity.

Additionally, a 500 h long-term test under *environmental condition (iv)* was conducted using a new batch of three cells sealed by method B. All of these devices were still working after the test, but showed significant degradation, maintaining only less than 5% of their initial efficiency. All photovoltaic parameters were reduced during aging, probably because of the gradual decomposition of the MAPbI<sub>3</sub> layer. The decrease in *FF* could also be arising from the gradual increase of the total series resistance of the cell, as shown in Figure 6, which was also measured in-situ during the aging test. A detailed post-mortem analysis of the degraded cells was conducted and the results are discussed in the following sections.

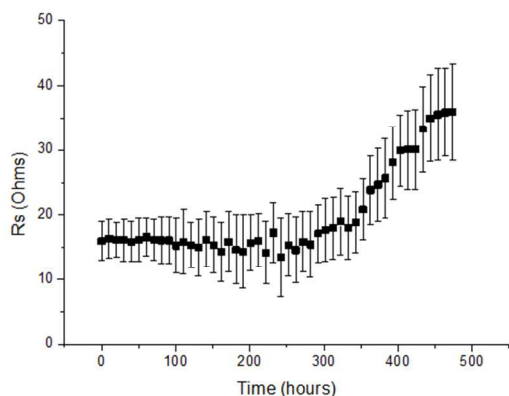


**Figure 6.** Gradual increase of the total series resistance of the cells tested at constant temperature (55 °C (85 °C)) and humidity (50%) under continuous one sun illumination (*environmental condition (iv)*). Resistance values from three devices were averaged and the error bars show the standard deviation.

### Investigation of the Degradation Pathways of Perovskite Solar Cells

For a post-mortem examination of the devices tested for 500 h at 55 °C (85 °C), the encapsulating cover glass was carefully removed without damaging the active photovoltaic area. From the back side it was visually evident that the most severely degraded area was the middle circular area of the silver layer that was directly exposed to illumination. The remaining area that was covered by a circular aperture (Figure 7) showed some damage but less severe. Under illumination, the uncovered area

would get significantly hotter than the covered area in the rest of the cell. The severer damage observed in the exposed circular area may be a result of combined thermal degradation and photodegradation.

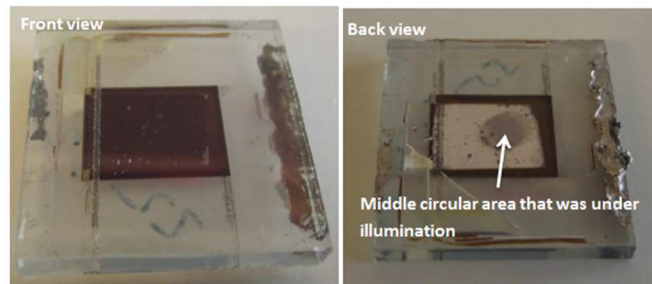


**Figure 7.** Photographs of a perovskite solar cell sealed with method B after 500 h of illumination at 55 °C (85 °C) and 50 % humidity (*conditions (iv)*). The encapsulating cover glass was removed for a better view.

After removal of the glass cover, cross-sectional FIB-SEM images of the degraded cell were taken (Figures 8 and 9). Compared to the new cells, a number of degradation features in the aged cell were evident: (a) damage and fragmentation of the silver layer; (b) voids formed in the Spiro-OMeTAD layer; (c) voids formed in the perovskite layer and detachment of the perovskite layer from the TiO<sub>2</sub> layer; (d) formation of new particles containing elements of high atomic numbers (brighter contrast in the SEM image) in the perovskite layer. Further analyses of the degraded devices are presented in the following sections.

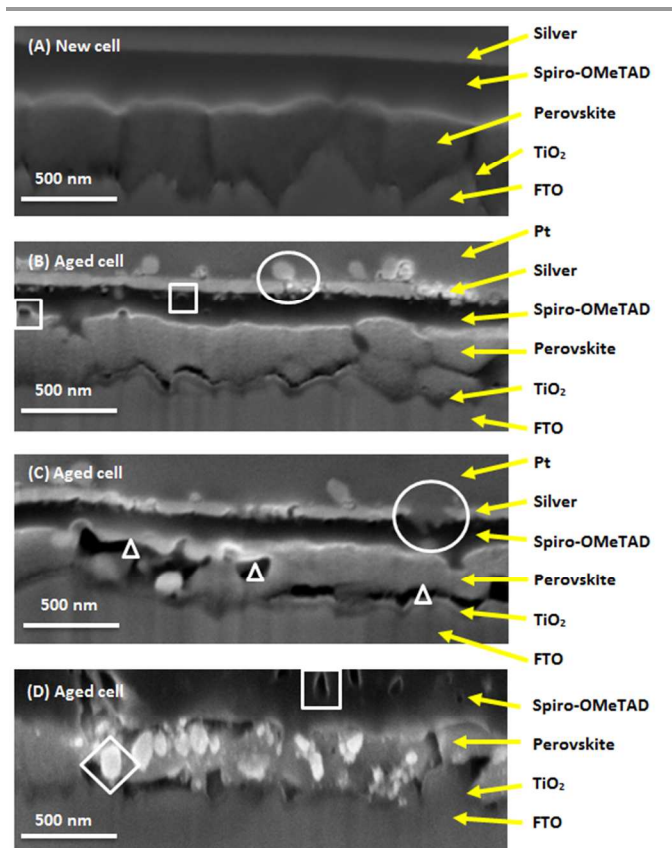


**Figure 8.** Cross-sectional FIB-SEM images of a new cell (A) and different areas of the aged cell (B-D) at constant temperature (55 °C (85 °C)) and humidity (50%) for 500 h. Degradation features are marked as follows: voids in the Spiro-OMeTAD layer (□); voids in the perovskite layer and detachment of the perovskite layer from the TiO<sub>2</sub> layer (Δ); damaged and discontinuous silver layer (○) and formation of particles with higher atomic numbers, likely PbI<sub>2</sub> (◊).

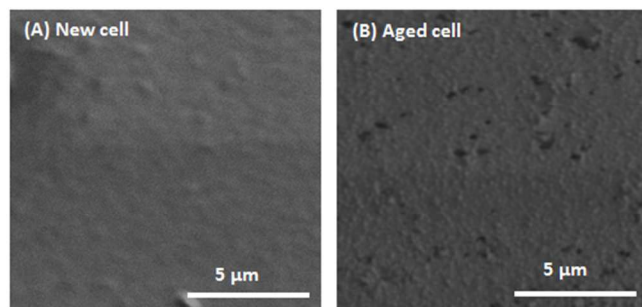


**Figure 9.** SEM images of the surface of the silver layer in a new (A) and an aged (B) perovskite solar cell that was tested at constant temperature (55 °C (85 °C)) and humidity (50%) for 500 h.

To analyse the causes of the microstructural changes observed in the SEM images of Figures 8 and 9, and to better understand the degradation pathways, additional samples with three different structures were prepared (Figure 10). Each new sample was designed to omit one of the functional layers in a normal solar cell device; sample **DA** was without the perovskite layer, **DB** without the Spiro-OMeTAD layer and **DC** without the Spiro-OMeTAD and silver layers. The samples were sealed using the sealing method B (Figure 2) and subsequently tested

at 55 °C (85 °C) and 50% humidity under 100 mW cm<sup>-2</sup> continuous illumination (*condition (iv)*) for 500 h in the environmental chamber. Afterwards, the samples were analysed and compared with the new devices using SEM and powder X-ray diffraction (XRD).

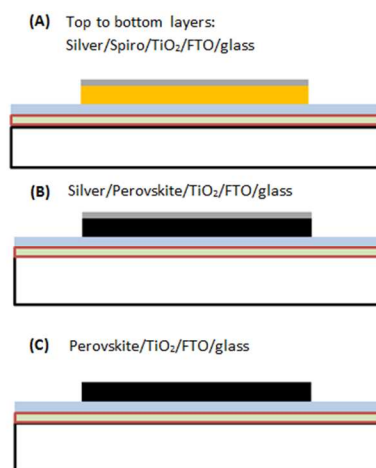


**Figure 10.** Design of samples with three different structures used for the aging tests; (A) Sample **DA** without a perovskite layer; (B) Sample **DB** without a Spiro-OMeTAD layer; (C) Sample **DC** with only the perovskite layer, all on a TiO<sub>2</sub> blocking layer coated FTO glass. All samples were encapsulated using the sealing method B illustrated in Figure 2.

In the perovskite free sample (**DA**) the microstructures of the silver, Spiro-OMeTAD, TiO<sub>2</sub> and FTO layers in both the new and aged cells showed almost no difference in the cross sectional images after the aging test (Figure 11 B and C). In addition, there was no evidence of degradation of the top Ag layer, from comparison of Figure 11A and Figure 9A. This indicated that Spiro-OMeTAD was stable in contact with silver and TiO<sub>2</sub> under *condition (iv)* (55 °C (85 °C), 50% humidity and 500 h). Thus, it can be concluded that the damages to the silver layer and the formation of voids in the Spiro-OMeTAD layer in the aged solar cell (Figures 8) were mainly associated with the degradation of the perovskite material at high temperature and humidity.

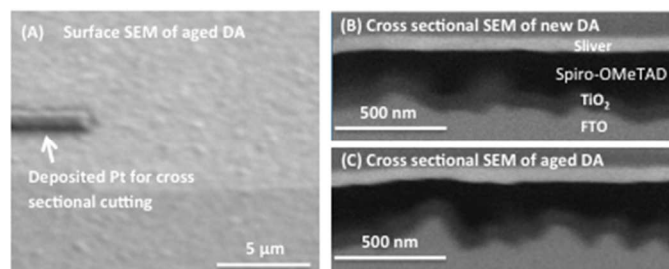


**Figure 11.** SEM images of the silver surface (A), and cross sections of new (B) and aged (C) devices for device **DA**, silver/ Spiro-OMeTAD/TiO<sub>2</sub>/FTO/glass structure after testing at 55 °C (85 °C), 50% humidity for 500 h.

In the sample without the Spiro-OMeTAD layer (sample **DB**), severe morphological changes were evident as a result of degradation of both the perovskite and silver layers after the

aging test (Figures 12 B and C). More precisely, the FIB cross-sectional SEM images in Figures 12 D and E show that the perovskite layer has changed dramatically. That is, a significant amount of it has shrunk to form lumps of residue, leaving voids in some areas after aging.

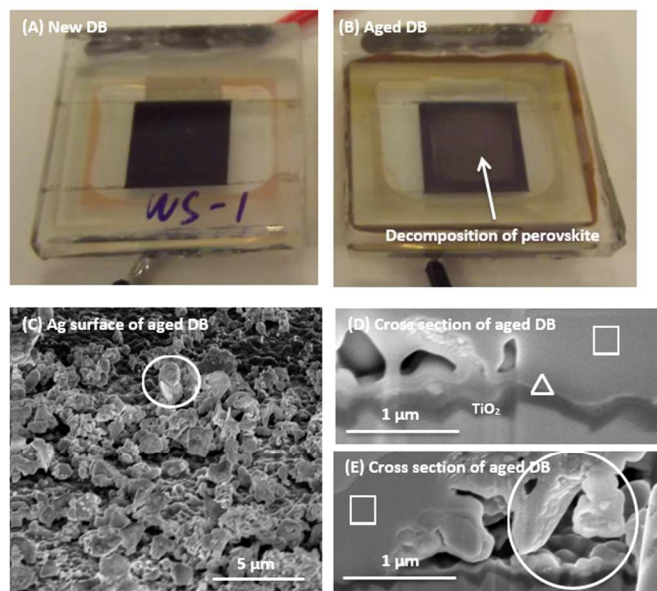


**Figure 12.** Photographs of the new and aged sample **DB** (Silver/Perovskite/TiO<sub>2</sub>/FTO/glass) before (A) and after (B) the aging test at 55 °C (85 °C), 50% humidity for 500 h; SEM images of the silver surface of the aged **DB** (C), cross section of the aged **DB** (D and E). The area where the perovskite layer totally disappeared is marked by (Δ) in (D); lump shaped degradation by-products and voids are marked by (○) in (C and E). Platinum layer deposited for Focused Ion Beam (FIB) cutting to reveal the cross section of the sample (□) was marked in (E).

To obtain more compositional information, powder XRD was used to analyse the surface of the new and aged **DB** samples (Figure 13). The XRD patterns showed that there was a clear reduction in the intensity of the Ag and MAPbI<sub>3</sub> perovskite diffraction peaks with the progression of aging, compared to the new sample. Furthermore, the diffraction peak (111) from γ-AgI<sup>31</sup> and the diffraction peak (001) from PbI<sub>2</sub><sup>15</sup> can be clearly observed in the aged samples and their intensities are shown to increase with time. Thus, it can be concluded that the Ag layer could be corroded through either the chemical reaction in direct contact with the perovskite layer or gaseous by-products, most likely HI, from the perovskite decomposition (see also reaction 2 in the introduction).<sup>21</sup> Hence, the lumps observed in the SEM image in Figures 12 C to E were likely corroded silver and PbI<sub>2</sub>. In a closed system like the solar cell encapsulated by method B, the reaction between silver and HI gas would continue until all of the Ag was consumed by HI or all the perovskite material was decomposed. This would result in a gradual increase of resistivity of the silver layer, as was observed in Figure 6.

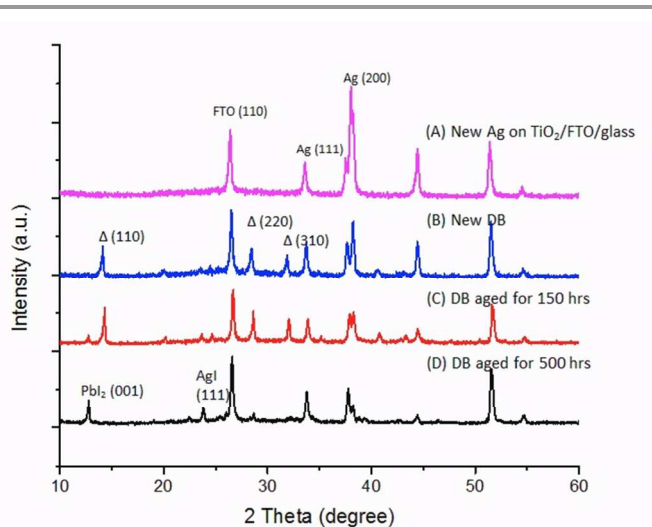


**Figure 13.** Powder XRD patterns of (A) new Ag coated on TiO<sub>2</sub>/FTO/glass; (B) new, (C) and (D) aged sample **DB** (Ag/perovskite/TiO<sub>2</sub>/FTO/glass) at 55 °C (85 °C), 50% humidity; (Δ) peaks from the CH<sub>3</sub>NH<sub>3</sub>PbI<sub>3</sub> perovskite phase.

Sample **DC** only had a perovskite layer coated on the TiO<sub>2</sub> blocking layer. There was almost no change in the dark colour of the perovskite layer after aging but an increase in grain size after aging was observed in the SEM images (Figure 14). From the powder XRD patterns, the (001) peak of PbI<sub>2</sub> can also be found in the aged **DC** sample (Figure 15). This showed that the decomposition of perovskite with ingress of water will occur when it is exposed to high temperature (85 °C in this work) but the degradation was not as severe as that observed in sample **DB** (Figure 12E). Therefore, it can be seen that the presence of silver is not beneficial to the stability of the perovskite solar cells.

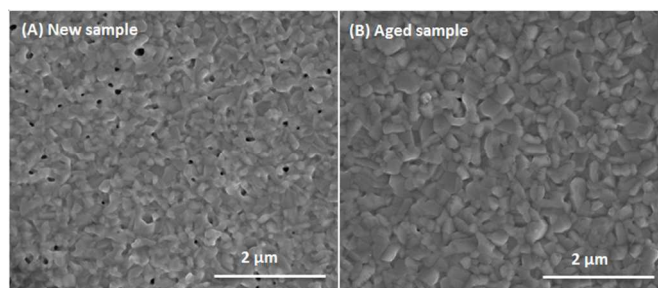


**Figure 14.** SEM images of the perovskite layer in Device **DC**, (A) new sample and (B) aged sample at 55 °C (85 °C), 50% humidity for 500 h.

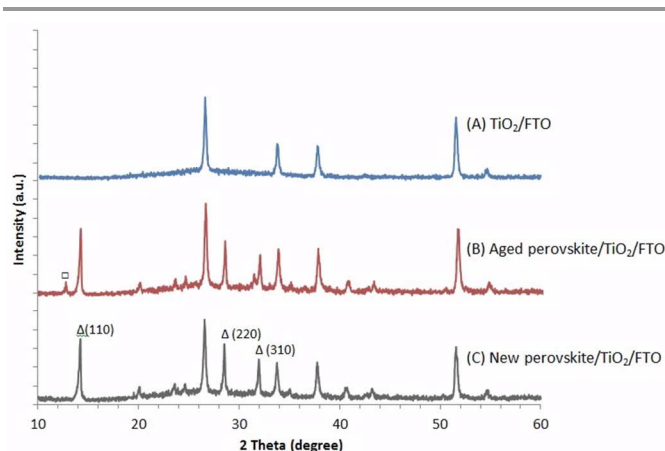


**Figure 15.** Powder XRD patterns for sample DC, (A)  $\text{TiO}_2$  on FTO glass; (B) aged sample of perovskite/ $\text{TiO}_2$ /FTO at 55 °C (85 °C), 50% humidity for 500 h; (C) a new sample of perovskite/ $\text{TiO}_2$ /FTO; ( $\Delta$ )  $\text{CH}_3\text{NH}_3\text{PbI}_3$  perovskite peaks; ( $\square$ ) (001) peak from  $\text{PbI}_2$ .

Thus, from the partially degraded perovskite solar cells in Figure 8 and the investigations of the three different configurations (**DA**, **DB**, **DC**), the following observations can be made:

- i. In an open system or not properly sealed environment (e.g., devices sealed by method A),  $\text{CH}_3\text{NH}_3\text{PbI}_3$  can decompose in the presence of water as a catalyst, forming  $\text{PbI}_2$ , and releasing gases such as HI and  $\text{CH}_3\text{NH}_2$  according to reactions (1) and (2). This process is accelerated by heat in the case of sealed solar cells as the sealing becomes more permeable. The release of the vapours will accelerate the decomposition reaction (according to reaction 2), so that given enough time,  $\text{CH}_3\text{NH}_3\text{PbI}_3$  will fully decompose into  $\text{PbI}_2$ .
- ii. In a closed system or properly sealed environment (e.g., devices sealed by method B),  $\text{CH}_3\text{NH}_3\text{PbI}_3$  decomposes at a slower rate (sample **DC**) due to less ingress of moisture through the sealing material. Although degradation is less severe and much slower in a properly sealed environment, the protecting material used is a desiccant and cannot consume the decomposition products of perovskite in this structure, namely HI and  $\text{CH}_3\text{NH}_2$ . Therefore, the vapour pressure of HI and/or  $\text{CH}_3\text{NH}_2$  increases and saturates the sealed environment. In such a situation, the perovskite decomposition reaction (2) reaches a dynamic equilibrium and thus the decomposition slows down significantly.
- iii. The voids observed in the Spiro-OMeTAD layer and perovskite layer are likely due to the release of gases from the decomposition of the perovskite material. As Spiro-OMeTAD is a softer material compared to the  $\text{TiO}_2$ /FTO/glass substrate, especially at high temperature, some

gases are trapped within the Spiro-OMeTAD layer, forming voids, and some reach the silver layer, causing corrosion of silver by HI, which eventually leads to the gradual increase of series resistance of the cell observed in Figure 7. Such reactions are severe when silver is directly deposited on top of the perovskite and are slowed down by the insertion of a Spiro-OMeTAD layer between the  $\text{CH}_3\text{NH}_3\text{PbI}_3$  and silver in a fully functioning perovskite solar cell. The presence of silver as a back contact will accelerate the degradation process as the silver will consume HI and shift the equilibrium of the decomposition reaction (2) to the right. The corrosive reaction will not stop until the entire  $\text{CH}_3\text{NH}_3\text{PbI}_3$  layer is decomposed or the entire silver layer is corroded. This also infers that the use of other materials that can react with acid, such as a ZnO blocking layer and/or ITO conductive layer, may also accelerate the perovskite degradation process. Thus, they would not be compatible with the  $\text{CH}_3\text{NH}_3\text{PbI}_3$  layer in PSCs.

iv.

Based on the investigations above, a scheme for the degradation processes of encapsulated  $\text{CH}_3\text{NH}_3\text{PbI}_3$  perovskite solar cells has been proposed and is depicted in Figure 16.

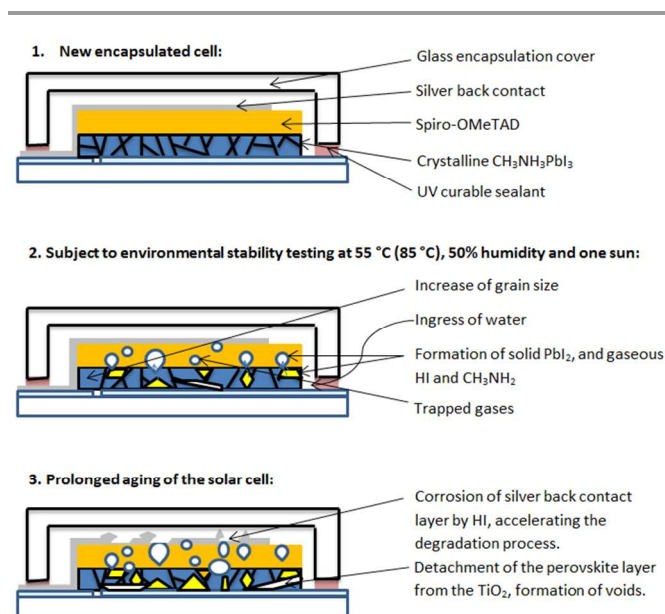


**Figure 16.** Scheme of the degradation processes of encapsulated methylammonium lead iodide perovskite solar cells illuminated at elevated temperatures and high humidity.

## Conclusions

The stability of planar methylammonium lead iodide perovskite solar cells at elevated temperature (up to 85 °C) and humidity (up to 80%) has been investigated. The encapsulated devices

showed good performance at room temperature and zero humidity, but degraded at high temperature and humidity. Improved stability was demonstrated by adopting a sealing technique from the OLED technology that effectively reduced the ingress of moisture into the cell at high temperature. From three purposely designed configurations, the degradation mechanism was analyzed using cross-sectional FIB-SEM and powder XRD analyses, and it was found that decomposition of the  $\text{CH}_3\text{NH}_3\text{PbI}_3$  phase became significant at  $85^\circ\text{C}$  in the presence of even a very small amount of water. A number of processes took place in conjunction with the perovskite decomposition: (i) corrosion of the thin silver layer and the formation of voids in the Spiro-OMeTAD layer by the gaseous products from the decomposition of the perovskite material; (ii) the formation of voids in the perovskite layer, plus detachment of the perovskite layer from the  $\text{TiO}_2$  layer and the formation of  $\text{PbI}_2$ . In a well encapsulated environment, the generated HI gas is consumed by reaction with the Ag, which promotes further decomposition of the perovskite material until the cell is fully degraded. Thus, replacement of the silver back contact by a chemically more stable conducting material, such as gold or carbonaceous materials, and selection of sealing materials that have better high temperature performance to further enhance the sealing/encapsulation of the devices are useful strategies to improve the stability of the perovskite solar cells at high temperatures and/or in the presence of water.

## Acknowledgement

The study was financially supported by the Australian Renewable Energy Agency, the Australian Centre for Advanced Photovoltaics and the Victorian State Government. YH is grateful for a Monash Graduate Scholarship. SM gratefully acknowledges the Alexander von Humboldt Foundation for a Feodor Lynen Fellowship. Electron microscopy access provided by the Monash University Centre for Electron Microscopy and the Advanced Microscopy Facility at The University of Melbourne are greatly acknowledged.

## Notes and references

<sup>a</sup> Australian Centre for Advanced Photovoltaics (ACAP), Department of Materials Engineering, Monash University, Victoria 3800, Australia

<sup>b</sup> Australian Centre for Advanced Photovoltaics (ACAP), School of Chemistry, Monash University, Victoria 3800, Australia

<sup>c</sup> PFPC, School of Chemistry, The University of Melbourne, Victoria 3010, Australia

<sup>d</sup> CSIRO Manufacturing Flagship, Bayview Ave, Clayton, Victoria 3168, Australia

<sup>e</sup> Australian Research Council Centre of Excellence for Electromaterials Science, Deakin University, Melbourne Burwood Campus, 221 Burwood Highway, Burwood, Victoria 3125, Australia

<sup>f</sup> Tech Fellow, The Melbourne Centre for Nanofabrication, 151 Wellington Road, Clayton 3168 Victoria, Australia

\* Corresponding authors. Email: [yibing.cheng@monash.edu](mailto:yibing.cheng@monash.edu), [leone.spiccia@moansh.edu](mailto:leone.spiccia@moansh.edu).

1. M. a. Green, A. Ho-Baillie, and H. J. Snaith, *Nat. Photonics*, 2014, **8**, 506–514.
2. N. J. Jeon, J. H. Noh, W. S. Yang, Y. C. Kim, S. Ryu, J. Seo, and S. Il Seok, *Nature*, 2015, **517**, 476–480.
3. A. Kojima, K. Teshima, Y. Shirai, and T. Miyasaka, *J. Am. Chem. Soc.*, 2009, **131**, 6051.
4. A. Kojima, K. Teshima, Y. Shirai, and T. Miyasaka, *J. Am. Chem. Soc.*, 2009, **131**, 6050–6051.
5. M. Grätzel, *Nat. Mater.*, 2014, **13**, 838–842.
6. M. Liu, M. B. Johnston, and H. J. Snaith, *Nature*, 2013, **501**, 395–398.
7. Q. Chen, H. Zhou, Z. Hong, S. Luo, H.-S. Duan, H.-H. Wang, Y. Liu, G. Li, and Y. Yang, *J. Am. Chem. Soc.*, 2014, **136**, 622–625.
8. A. Yella, L.-P. Heiniger, P. Gao, M. K. Nazeeruddin, and M. Grätzel, *Nano Lett.*, 2014, **14**, 2591–2596.
9. M. Xiao, F. Huang, W. Huang, Y. Dkhissi, Y. Zhu, J. Etheridge, A. Gray-Weale, U. Bach, Y.-B. Cheng, and L. Spiccia, *Angew. Chemie*, 2014, **126**, 10056–10061.
10. F. Huang, Y. Dkhissi, W. Huang, M. Xiao, I. Benesperi, S. Rubanov, Y. Zhu, X. Lin, L. Jiang, Y. Zhou, A. Gray-Weale, J. Etheridge, C. R. McNeill, R. A. Caruso, U. Bach, L. Spiccia, and Y.-B. Cheng, *Nano Energy*, 2014, **10**, 10–18.
11. J.-H. Im, C.-R. Lee, J.-W. Lee, S.-W. Park, and N.-G. Park, *Nanoscale*, 2011, **3**, 4088–4093.
12. I. Chung, B. Lee, J. He, R. P. H. Chang, and M. G. Kanatzidis, *Nature*, 2012, **485**, 486–489.
13. H.-S. Kim, C.-R. Lee, J.-H. Im, K.-B. Lee, T. Moehl, A. Marchioro, S.-J. Moon, R. Humphry-Baker, J.-H. Yum, J. E. Moser, M. Grätzel, and N.-G. Park, *Sci. Rep.*, 2012, **2**, 591.
14. M. M. Lee, J. Teuscher, T. Miyasaka, T. N. Murakami, and H. J. Snaith, *Science*, 2012, **338**, 643–647.
15. J. Burschka, N. Pellet, S.-J. Moon, R. Humphry-Baker, P. Gao, M. K. Nazeeruddin, and M. Grätzel, *Nature*, 2013, **499**, 316–319.
16. M. A. Green, K. Emery, Y. Hishikawa, W. Warta, and E. D. Dunlop, *Prog. Photovoltaics Res. Appl.*, 2013, **21**, 827–837.
17. T. Leijtens, G. E. Eperon, S. Pathak, A. Abate, M. M. Lee, and H. J. Snaith, *Nat. Commun.*, 2013, **4**, 2885.
18. J. H. Noh, S. H. Im, J. H. Heo, T. N. Mandal, and S. Il Seok, *Nano Lett.*, 2013, **13**, 1764–1769.
19. W. Li, H. Dong, L. Wang, N. Li, X. Guo, J. Li, and Y. Qiu, *J. Mater. Chem. A*, 2014, **2**, 13587–13592.
20. a. Mei, X. Li, L. Liu, Z. Ku, T. Liu, Y. Rong, M. Xu, M. Hu, J. Chen, Y. Yang, M. Grätzel, and H. Han, *Science*, 2014, **345**, 295–298.
21. J. M. Frost, K. T. Butler, F. Brivio, C. H. Hendon, M. van Schilfgaarde, and A. Walsh, *Nano Lett.*, 2014, **14**, 2584–2590.
22. W. F. Giaque and R. Wiebe, *J. Am. Chem. Soc.*, 1929, **51**, 1441–1449.
23. J. G. Aston, C. W. Siller, and G. H. Messerly, *J. Am. Chem. Soc.*, 1937, **59**, 1743–1751.
24. D. C. Jordan and S. R. Kurtz, *Prog. Photovoltaics Res. Appl.*, 2013, **21**, 12–29.
25. E. Cuddihy, C. Coulbert, A. Gupta, and R. Liang, *JPL Publ.*, 1986, **VII**, 86–31.

26. M. C. Alonso García and J. L. Balenzategui, *Renew. Energy*, 2004, **29**, 1997–2010.
27. J. Burschka, A. Dualeh, F. Kessler, E. Baranoff, N.-L. Cevey-Ha, C. Yi, M. K. Nazeeruddin, and M. Grätzel, *J. Am. Chem. Soc.*, 2011, **133**, 18042–18045.
28. M. O. Reese, S. a. Gevorgyan, M. Jørgensen, E. Bundgaard, S. R. Kurtz, D. S. Ginley, D. C. Olson, M. T. Lloyd, P. Morvillo, E. a. Katz, A. Elschner, O. Haillant, T. R. Currier, V. Shrotriya, M. Hermenau, M. Riede, K. R. Kirov, G. Trimmel, T. Rath, O. Inganäs, F. Zhang, M. Andersson, K. Tvingstedt, M. Lira-Cantu, D. Laird, C. McGuinness, S. (Jimmy) Gowrisanker, M. Pannone, M. Xiao, J. Hauch, R. Steim, D. M. DeLongchamp, R. Rösch, H. Hoppe, N. Espinosa, A. Urbina, G. Yaman-Uzunoglu, J.-B. Bonekamp, A. J. J. M. van Breemen, C. Girotto, E. Voroshazi, and F. C. Krebs, *Sol. Energy Mater. Sol. Cells*, 2011, **95**, 1253–1267.
29. Y. Yamada, M. Endo, A. Wakamiya, and Y. Kanemitsu, *J. Phys. Chem. Lett.*, 2015, 482–486.
30. Y. Kawamura, H. Mashiyama, and K. Hasebe, *J. Phys. Soc. Japan*, 2002, **71**, 1694–1697.
31. M. Vukic, D. Veselinovic, and V. Markovic, *J. Serbian Chem. Soc.*, 2007, **72**, 857–868.